

Combination of Thresholding and Otsu Method in Increasing Results of Identification of Malaria Parasite Type in Thin Blood Smear Image

Rika Rosnelly, Jani Kusanti, Linda Wahyuni and Suparni

Abstract---Separation of objects that is not optimal affects the results of subsequent image calculations and greatly affects the accuracy of the identification results. Various methods are used to separate objects (foreground) and background (background), especially in the parasitic image that is on the image of a smear of red blood cells. However, the thresholding method has not been able to optimally separate objects in the malaria parasite image to identify the type of malaria parasite because determining the pixel values for the threshold is done manually, so the identification process shows results that are less than the maximum accuracy. This research is very important by combining the thresholding method with the otsu method to improve the results of identification of malaria parasites based on digital image processing. Otsu determines the pixel for the threshold automatically using a determinant. To identify using four criteria: area, perimeter, mean intensity, and eccentricity. The results showed that the combination of thresholding - Otsu was superior compared to the performance of the thresholding method. The results of the binary value calculation on the combination of the Otsu thresholding method produce higher accuracy values than the thresholding method. Thus, the combination of the Otsu thresholding method can be used as a proposed segmentation method for the identification of malaria parasite types based on digital image processing.

Keywords---Segmentation, Otsu, Thresholding, Malaria.

I. INTRODUCTION

The health ministry said malaria cases in Indonesia reached 70 percent of them in the eastern region. Eastern Indonesia has a malaria prevalence of more than 400,000 cases. The prevalence of malaria in Indonesia in 2017 reached 417,819 positive cases[1][2]. We need to realize that malaria is never separated from humans, we need to be careful to avoid this type of tropical disease[3]. Techniques to identify malaria have been carried out by several researchers [4][5][6][7][8][9]. The segmentation process is done by improving image quality[10] and thresholding[4][11][12][13][14] to isolate an object completely, the conditions of both the object and background vary.

Thresholding uses one pixel value that is manually determined to determine the threshold results [15][16]. The results obtained are not as expected, because not all malaria parasitic images can be isolated from the background image. Research on the identification of malaria has been carried out using the thresholding method, the otsu method [4]. The study of malaria parasites that used a combination of thresholding methods and otsu methods which conducted by previous researchers are still rare. Therefore, they need to obtain the thresholding method and the otsu method so that the thresholding method and the otsu method are more complete.

Rika Rosnelly, Universitas Potensi Utama, Engineering and Computer Sciences Faculty. E-mail: rikarosnelly@gmail.com
Jani Kusanti, Universitas Surakarta, Fakultas Teknik Elektro dan Informatika. E-mail: linda@potensi-utama.ac.id
Linda Wahyuni, Universitas Potensi Utama, Engineering and Computer Sciences Faculty. E-mail: jani_kusanti@yahoo.com
Suparni, Politeknik Kesehatan Kemenkes Medan. E-mail: hajjahsuparni@gmail.com

In order to overcome this problem, this research built a model using a combination of thresholding method with otsu method and obtains the results of identification of malaria types and stages based on the image of malaria parasite thin blood smear so as to determine falciparum, malariae and vivax with ring, trophozoite, schizont and gametocyte stages.

The results of this study identify the types of malaria and its stadium based on the image of the malaria parasite thin blood smear by combining the method thresholding with the Otsu method so that it is more optimal.

Otsu is a global thresholding [17][18], conducting discriminant analysis to determine variables that distinguish between two or more groups that arise naturally. Discriminant analysis [20][21][22] is used to maximize these variables so that they can divide foreground and background objects automatically.

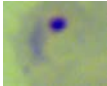
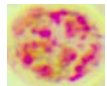
The Canny method is used to localize pixel points on the edge[23][24][25][26] to eliminate noise. This method is done to increase edge strength[26][27]. The smoothing of the noise is done by the four angles of 00, 450, 900 and 1350. Pixels that are not considered to be edges are changed to 0.

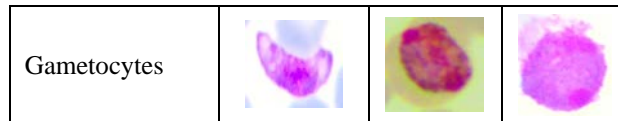
[28][29][30][31]classification is done for image identification. The use of artificial neural networks is carried out in the classification process [32][32]. In the back propagation process, adjusting each weight and bias is based on the error value obtained at the forward pass. The way the back propagation process works is known as a multilayer neural network. In the calculation process, the gradient descent method is used to minimize the error of the total square of the output calculated by the network. The combination of the thresholding method with the otsu method is proposed to optimize the accuracy of the image results. The thresholding method and the otsu method will be combined to improve the results of a more optimal accuracy in identifying the types of malaria parasites and their staging on thin blood smear images.

II. METHOD

This study uses malaria parasitic images on thin blood smear images, as many as 120 training image data and, 30 test data images. The malaria parasite used consisted of falciparum, malariae and vivax with each type having a ring stage, trophozoite, schizont and gametocytes can be shown in Table 1. [7].

Table 1: Types of Malaria Parasites and Stadium

Parasite Stadium	Class		
	Falciparum	Malariae	Vivax
Ring			
Trophozoite			
Schizont			



The use of a thresholding value at one pixel point makes the results not optimal as shown in the equation 1,[19]

$$f_0(x, y) = \begin{cases} 0, & f_1(x,y) < 128 \\ 255, & f_1(x,y) \geq 128 \end{cases} \quad [1]$$

Shown in Fig. 1 image of the 8x8 pixel malaria parasite,

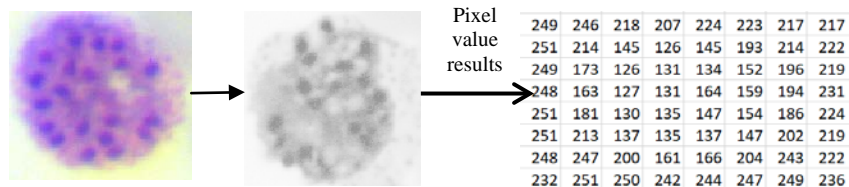


Figure 1: Example of a parasite image pixel size of 8x8

With reference to equation 1, the calculation results are shown in Fig. 2,

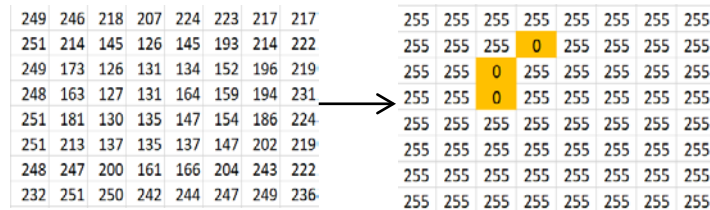


Figure 2: The result of calculating one-pixel value 128

The results of the thresholding calculation in Fig. 2 can be seen that the image results are less than optimal, where for 120 training data the 64% accuracy level is generated with a mean square error (MSE) of 9,66667.

The Otsu method looks for a threshold value (T) with discriminant analysis on a variable that can distinguish between two or more groups that arise naturally. The threshold value of otsu is expressed as k, the value of k is between 1-L, with L = 255. The calculation starts from equation 2,

$$p(i) = \frac{n_i}{N}, p(i) \geq 0, \sum_1^{256} p(i) = 1 \quad (2)$$

$p(i)$ = histogram value, N = the sum of all n_i starting from n_0 to n_{L-1} , n_i = number of pixels at each intensity. So it can be concluded, $0 \leq p(i) < 1$. In this study otsu is divided into background (wB) and image objects (wO), the calculation is shown in equation 3 and equation 4,

$$wB(k) = \sum_{i=1}^k p(i) \quad (3)$$

Equation 3, $wB(k)$ is the background weight to find the cumulative number of kth histogram values, with k= 0, 1, 2 ...L-1

$$wO(k) = N - \omega B(k) \quad (4)$$

Equation 4, $wO(k)$ is the result of the sum of all the matrices minus the cumulative sum of kth histogram values.

$$jum_B(k) = \sum_{i=1}^k i * p(i) \quad (5)$$

Equation 5, the sum of all kth pixels, $jum_B(k)$, for $k= 0, 1, 2 \dots L-1$

$$mB(k) = \frac{jum_B(k)}{wB(k)} \quad (6)$$

Equation 6, average background yield, $mB(k)$ is the total number of ith pixels divided by the background weight for $k= 0, 1, 2, \dots L-1$

$$mF(k) = \frac{jum_Tot(k) - jum_B(k)}{wO(k)} \quad (7)$$

Equation 7, average foreground results, $mF(k)$ is the total number of pixels for $k= 0, 1, 2, \dots L-1$ minus the total number of it pixels divided by the number of foreground weights, for the value of variance (k) can be seen equation 8,

$$Var(k) = wB(k) * wO(k) * (mB(k) - mF(k))^2 \quad (8)$$

The result of the threshold value is used for image segmentation. The optimum threshold value is used by otsu. The segmentation equation is shown in equation 9,

$$g(x, y) = \begin{cases} 1 & \text{if } f(x, y) > k^* \\ 0 & \text{if } f(x, y) \leq k^* \end{cases} \quad (9)$$

The results of segmentation are binary images with 0 and 1. intensity values are 0 for black and 1 for white (as an object).

To optimize the measurement results on the image, the otsu results are processed using canny edge detection, this process uses a Gaussian derivative kernel. Because otsu is already in the thresholding process, in the canny process the next stage determines the final edge by pressing all sides that are not connected to the very strong edges. G_x and G_y results from otsu are used as gradients in the x and y directions, respectively.

Large gradients show fairly clear edges. However, the edges are usually broad, unable to show where the actual edges are. To determine the actual edge, the edge angle must be determined and stored as shown in equation 10,

$$\theta = \arctan\left(\frac{|G_y|}{|G_x|}\right) \quad (10)$$

G_x and G_y , is the x and y direction gradient, the next step is to convert the blurred edges in the image of the magnitude gradient to produce sharp edges. This is done by maintaining all local maxima in the gradient image and erasing everything else.

The algorithm for each pixel in the gradient image is shown in Fig. 3:

- Rotate the gradient direction θ to the nearest 45° , then connect with the 8 neighboring points connected to it.
- Compare the current edge pixel value with the edge pixel value in the positive and negative direction of the gradient. If the gradient's direction is north ($\theta = 90^\circ$), compare it with pixels north and south.
- If the current edge pixel value is the largest, then save the edge value, but if not, delete the value.

Figure 3: Canny's edge detection algorithm

Edge pixels remaining after non-maximum removal are indicated by a strong pixel-by-pixel value. The simplest way to differentiate is to use a threshold value so that only edges with strong values will be retained. Here the Canny algorithm uses a double thresholding system where edges with values greater than the upper threshold are marked as strong points, edges with values smaller than the lower threshold will be removed, and edges with pixel values between the upper threshold and the lower threshold will be marked as edges the weak.

To get the area, perimeter, eccentricity, and metric variables used as input values, the equation is shown 11-14,[19]

$$Area = \sum_x \sum_y f(x, y) \quad (11)$$

$$Perimeter = \sum_x \sum_y f(x, y), x, y \in Boundary\ region \quad (12)$$

$$eccentricity = \sqrt{1 - \frac{b^2}{a^2}} \quad (13)$$

$$metric = \frac{4\pi * A}{c^2} \quad (14)$$

The classification used in this study uses a backpropagation model, the algorithm shown in Fig. 4, [33][34]

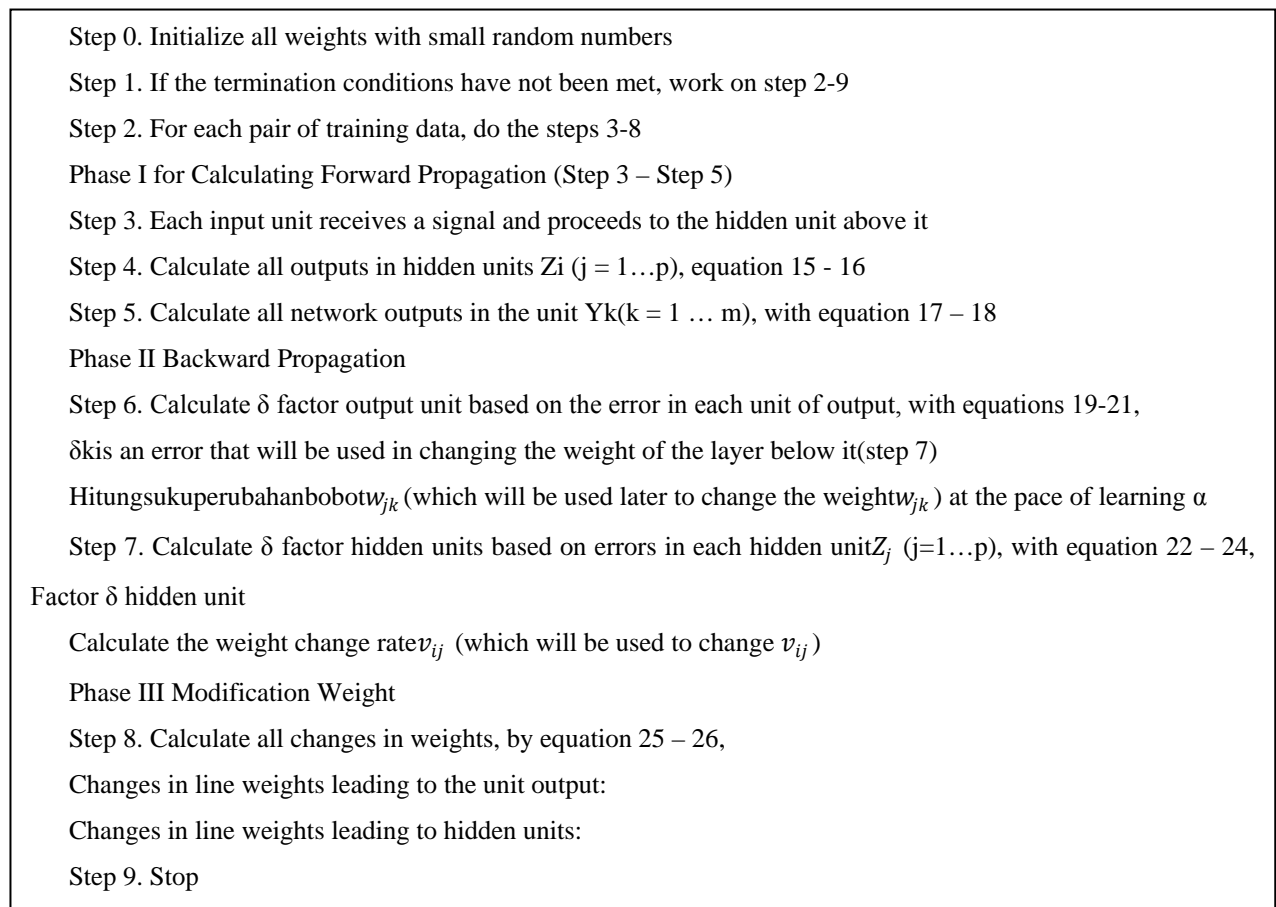


Figure 4: The algorithm calculates forward propagation

$$Z_{net\ j} = V_{0j} + \sum_{i=1}^p X_i V_{ij} \quad (15)$$

$$Z_j = f(Z_{-net\ j}) = \frac{1}{1+e^{-z_{net\ j}}} \quad (16)$$

$$Y_{-net\ k} = w_{0j} + \sum_{k=1}^m Z_j W_{jk} \quad (17)$$

$$y_k = f(Y_{net\ k}) = \frac{1}{1+e^{-y_{net\ k}}} \quad (18)$$

$$Y_k (k = 1, 2, \dots, m) \quad (19)$$

$$\delta_k = (t_k - y_k) f(y_{-net\ k}) = (t_k - y_k) y_k (1 - y_k) \quad (20)$$

$$\Delta W_{jk} = \alpha \delta_k Z_j \quad (k = 1, 2, \dots, m; j = 0, 1, 2, \dots, p) \quad (21)$$

$$\delta_{-net\ j} = \sum_{k=1}^m \delta_k W_{jk} \quad (22)$$

$$\delta_j = \delta_{-net\ j} f(Z_{-net\ j}) = \delta_{net\ j} Z_j (1 - Z_j) \quad (23)$$

$$\Delta V_{ij} = \alpha \delta_j X_j \quad (j = 1, 2, \dots, p; i = 0, 1, 2, \dots, n) \quad (24)$$

$$w_{jk} (baru) = w_{jk} (lama) + \Delta w_{jk} \quad (k = 1, 2, \dots, m; j = 0, 1, 2, \dots, p) \quad (25)$$

$$v_{ij} (baru) = v_{ij} (lama) + \Delta v_{ij} \quad (j = 1, 2, \dots, p; i = 0, 1, 2, \dots, n) \quad (26)$$

During the forward propagation process, the input signal (xi) is propagated to the hidden layer using the specified activation function. Output from each hidden layer unit (zj) to produce network output (yk). Next, the network output (yk) is compared with the target to be achieved (tk). Difference tk - yk is an error that occurs. If the error < of the tolerance limit, the weight of each line in the network is modified to reduce errors that occur.

III. RESULTS AND DISCUSSION

In the initial stage the preprocessing process is carried out on the image of the cropping results, the same process is carried out on the same three tests, shown in Fig. 5

Initial Imagery	Method			
	Grayscale	Thresholding	Otsu	Thresholding+Otsu
				
183 159 163 191 167 144 159 178 197 166 181 197 232 216 197 192				
151 105 116 169 117 88 103 142 173 114 142 184 245 216 190 188	169 133 140 180 142 116 129 157 183 138 158 188 237 214 192 190	1 1 1 1 1 0 1 1 1 1 1 1 1 1 1 1	0 0 0 1 0 0 0 0 1 0 0 1 1 1 1 1	1 0 0 1 0 0 0 0 1 0 0 1 1 1 1 1
222 208 199 210 206 191 186 183 199 185 184 188 211 198 192 196				

Figure 5: Calculation results for each method

Calculation results are shown in Fig. 6 and Fig. 7:

((183*0,299)+(151+0,587)+(222*0,144))	((159*0,299)+(105+0,587)+(208*0,144))	((163*0,299)+(116+0,587)+(199*0,144))	((191*0,299)+(169+0,587)+(210*0,144))
((167*0,299)+(117+0,587)+(206*0,144))	((144*0,299)+(88+0,587)+(191*0,144))	((159*0,299)+(103+0,587)+(1186*0,144))	((178*0,299)+(142+0,587)+(183*0,144))
((197*0,299)+(173+0,587)+(199*0,144))	((166*0,299)+(114+0,587)+(185*0,144))	((181*0,299)+(142+0,587)+(184*0,144))	((197*0,299)+(184+0,587)+(188*0,144))
((232*0,299)+(245+0,587)+(211*0,144))	((216*0,299)+(216+0,587)+(198*0,144))	((197*0,299)+(190+0,587)+(192*0,144))	((192*0,299)+(188+0,587)+(196*0,144))

Figure 6: Calculation of RGB to grayscale

The result:

169	133	140	180
142	116	129	157
183	138	158	188
237	214	192	190

Figure 7: Grayscale Results

For all values of $f(x, y)$ greater than 128, the value becomes 1, and for all values of $f(x, y)$ smaller than 128, the value becomes 0, the result of thresholding is shown in Fig. 8,

169>128	133>128	140>128	180>128	=	1	1	1	1
142>128	116<128	129>128	157>128		1	0	1	1
183>128	138>128	158>128	188>128		1	1	1	1
237>128	214>128	192>128	190>128		1	1	1	1

Figure 8: Results from grayscale to thresholding

Calculation results for otsu, shown in Fig. 9,

169	133	140	180	→	0	0	0	1
142	116	129	157		0	0	0	0
183	138	158	188		1	0	0	1
237	214	192	190		1	1	1	1

Figure 9: Results from grayscale to otsu

Calculation results for thresholding + otsu, shown in Fig. 10,

169	133	140	180	→	1	0	0	1
142	116	129	157		0	0	0	0
183	138	158	188		1	0	0	1
237	214	192	190		1	1	1	1

Figure 10: Results from grayscale to thresholding+otsu

The calculation results of the three methods obtained by the value of thresholding with thresholding + otsu many differences, while the results of otsu with thresholding + otsu obtained results that are not much different. The results of each calculation are processed to obtain characteristic values based on area, metric, perimeter and eccentricity. The differences in the results of the three are shown in Table 2.

Table 2: Comparison table of the results of the calculation of the characteristics for the training data

Thresholding	Area			Metric			Perimeter			Eccentricity		
	Otsu	Gabung	Thresholding	Otsu	Thresholding + Otsu	Thresholding	Otsu	Gabung	Thresholding	Otsu	Gabung	
58669	42999	42999	0,70863	0,5194	0,519359	1.020	1.020	1.020	0,03143	0,192	0,1921	
48405	60842	60842	0,10997	0,7349	0,734874	2.352	1.020	1.020	0,54425	0,159	0,1592	
61635	62548	62548	0,74445	0,7555	0,75548	1.020	1.020	1.020	0,11169	0,105	0,1053	
60953	59871	59871	0,73621	0,7231	0,723146	1.020	1.020	1.020	0,21157	0,24	0,2405	
41197	41498	41498	0,49759	0,5012	0,50123	1.020	1.020	1.020	0,19078	0,186	0,186	
46300	52462	52462	0,55923	0,6337	0,633657	1.020	1.020	1.020	0,21498	0,177	0,1775	
57245	58427	58427	0,69143	0,7057	0,705705	1.020	1.020	1.020	0,2037	0,191	0,1908	
49812	51437	51437	0,10187	0,2213	0,221282	2.479	1.709	1.709	0,42631	0,403	0,4031	
49013	50900	50900	0,592	0,6148	0,614791	1.020	1.020	1.020	0,24346	0,217	0,2171	
53676	55633	55633	0,64832	0,672	0,671958	1.020	1.020	1.020	0,36956	0,339	0,3386	
34692	38724	38724	0,41902	0,4677	0,467724	1.020	1.020	1.020	0,25858	0,247	0,2472	
32961	47449	47449	0,13401	0,5731	0,573108	1.758	1.020	1.020	0,64314	0,372	0,3717	
49279	49926	49926	0,32451	0,4326	0,432647	1.381	1.204	1.204	0,28114	0,269	0,2686	
46530	56851	56851	0,1305	0,6588	0,658847	2.117	1.041	1.041	0,3643	0,305	0,3047	
37572	45513	45513	0,45381	0,5497	0,549724	1.020	1.020	1.020	0,33974	0,299	0,2987	
37572	45513	45513	0,45381	0,5497	0,549724	1.020	1.020	1.020	0,33974	0,299	0,2987	
61154	61784	61784	0,73864	0,7463	0,746252	1.020	1.020	1.020	0,16488	0,155	0,155	
63541	63372	63921	0,76747	0,7654	0,772064	1.020	1.020	1.020	0,08697	0,09	0,0788	
53676	55633	55633	0,64832	0,672	0,671958	1.020	1.020	1.020	0,36956	0,339	0,3386	
63351	63405	63405	0,76518	0,7658	0,765831	1.020	1.020	1.020	0,16604	0,163	0,1633	
49928	50340	50340	0,60305	0,608	0,608027	1.020	1.020	1.020	0,27041	0,267	0,2669	
55767	57352	57352	0,67358	0,6927	0,692721	1.020	1.020	1.020	0,22763	0,203	0,2027	
32779	34760	34760	0,39592	0,4198	0,419845	1.020	1.020	1.020	0,44022	0,404	0,4043	
62861	36935	36935	0,75926	0,4461	0,446116	1.020	1.020	1.020	0,18562	0,314	0,3135	
50948	55925	55925	0,40599	0,6755	0,675485	1.256	1.020	1.020	0,28705	0,31	0,3104	
52014	53396	53396	0,62825	0,6449	0,644938	1.020	1.020	1.020	0,37045	0,351	0,3512	
30700	35721	35721	0,17781	0,1212	0,1212	1.473	1.924	1.924	0,7185	0,411	0,4113	
44325	48584	48584	0,53538	0,5868	0,586817	1.020	1.020	1.020	0,21976	0,164	0,164	
33489	34568	34568	0,40449	0,4175	0,417526	1.020	1.020	1.020	0,41169	0,414	0,414	
38988	42447	42447	0,47091	0,5127	0,512692	1.020	1.020	1.020	0,37089	0,349	0,3492	

Table 2. is a sample of the results from the calculation of the characteristics of the training data. The number of training data is 120 image data of malaria parasite species consisting of falciparum malaria parasites, malariae and vivax along with stages, namely rings, trophozoites, schizonts and gametocytes. The results of the training using the thresholding method obtained an accuracy value of 75%, using the otsu method obtained 91% results, while for the training results using the combination of thresholding + otsu obtained an accuracy value of 100%.

The results of the training using the thresholding method and the thresholding + otsu method are shown in Fig. 11 and Fig. 12

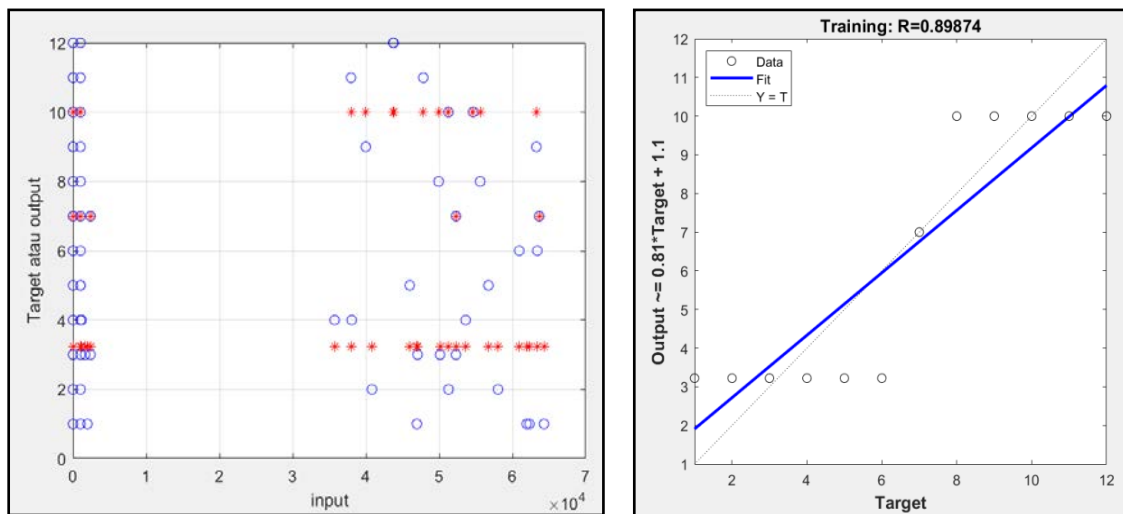


Figure 11: The results of backpropagation classification of training data using the thresholding method

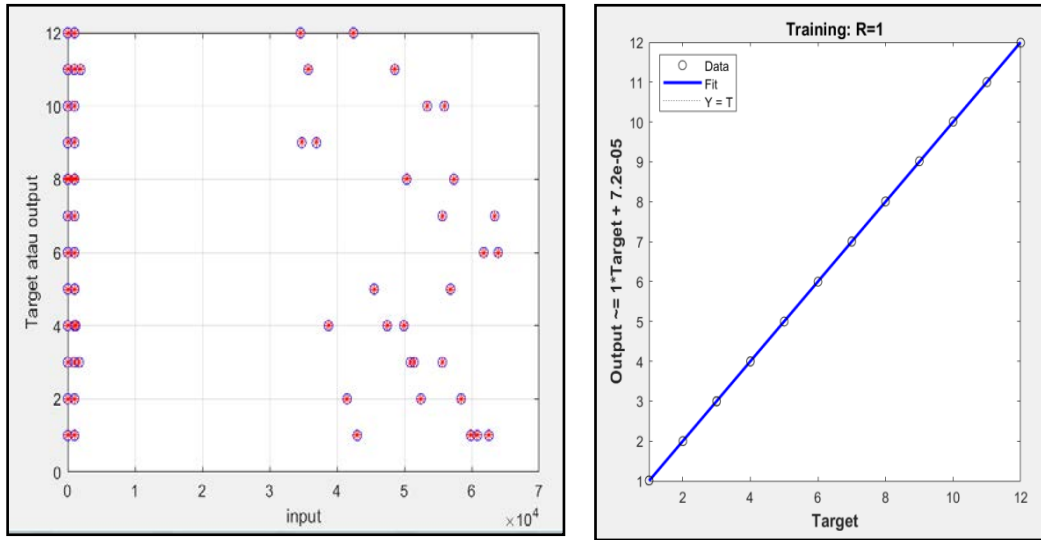


Figure 12: Results of backpropagation classification of training data from the thresholding + otsu method

The test results for identification using 30 test data, using the thresholding, otsu, thresholding + otsu methods are shown in Fig. 13

	Thresholding						Otsu						Thresholding+Otsu					
	Area	Metric	Perimeter	Eccentricity	T	H	Area	Metric	Perimeter	Eccentricity	T	H	Area	Metric	Perimeter	Eccentricity	T	H
	63935	0,77223	1020	0,081377	FR	MR	62548	0,75548	1020	0,10526	FR	FR	62548	0,75548	1020	0,10526	FR	FR
	61853	0,74709	1020	0,17861	FR	FR	59871	0,72315	1020	0,24046	FR	FR	59871	0,72315	1020	0,24046	FR	FR
	45013	0,54369	1020	0,11811	FZ	FT	41498	0,50123	1020	0,18597	FS	FS	41498	0,50123	1020	0,18597	FS	FS
	51058	0,6167	1020	0,18806	FZ	FZ	52462	0,63366	1020	0,1775	FS	FS	52462	0,63366	1020	0,1775	FS	FS
	10843	0,13097	1020	0,54791	FT	FS	51437	0,22128	1709	0,40308	FT	FT	51437	0,22128	1709	0,40308	FT	FT
	16263	0,19463	1020	0,74747	FT	GF	50900	0,61479	1020	0,21708	FT	FT	50900	0,61479	1020	0,21708	FT	FT
	5654	0,068291	1020	0,6634	FT	GF	55633	0,67196	1020	0,33863	FT	FT	55633	0,67196	1020	0,33863	FT	FT
	35661	0,43073	1020	0,25507	GF	GF	38724	0,46772	1020	0,24724	GF	GF	38514	0,46519	1020	0,2471	GF	GF
	39000	0,47106	1020	0,37445	GF	GF	47449	0,57311	1020	0,37175	GF	GF	47449	0,57311	1020	0,37175	GF	GF
	57897	0,6993	1020	0,15563	GF	GF	49926	0,43265	1204	0,26863	GF	GF	49926	0,43265	1204	0,26863	GF	GF
	56403	0,68126	1020	0,31137	MG	MG	56851	0,65885	1041	0,30471	MG	FR	56851	0,65885	1041	0,30471	GF	VS
	51280	0,61938	1020	0,27227	MG	MG	45513	0,54972	1020	0,29874	MG	MG	45513	0,54972	1020	0,29874	MG	MG
	51282	0,6194	1020	0,27221	MG	MG	45513	0,54972	1020	0,29874	MG	GF	45513	0,54972	1020	0,29874	MG	VS
	5738	0,069306	1020	0,85512	MR	MG	61784	0,74625	1020	0,15496	MR	MR	61764	0,74625	1020	0,15496	MR	FR
	14509	0,17525	1020	0,79956	MR	MG	60390	0,72622	1022	0,10318	MR	FR	63921	0,77206	1020	0,07875	MR	FR
	53908	0,65112	1020	0,22902	MS	MT	54107	0,65353	1020	0,22762	MS	GF	54107	0,65353	1020	0,22762	MS	MS
	62124	0,75036	1020	0,084965	MS	MT	61363	0,74117	1020	0,087545	MS	MT	61363	0,74117	1020	0,087545	MS	MS
	5654	0,068291	1020	0,6634	MS	GF	55633	0,67196	1020	0,33863	MS	FT	55633	0,67196	1020	0,33863	MS	FT
	62837	0,75897	1020	0,25992	MT	FR	53024	0,64045	1020	0,38706	MT	MT	53024	0,64045	1020	0,38706	MT	MT
	58227	0,70329	1020	0,2154	MT	MG	54567	0,65908	1020	0,27506	MT	MT	54567	0,65908	1020	0,27506	MT	MT
	41951	0,5067	1020	0,25535	MT	MG	41163	0,49718	1020	0,26208	MT	MG	41163	0,49718	1020	0,26208	MT	VR
	61524	0,74311	1020	0,23465	VR	FR	55925	0,67548	1020	0,31042	VR	VR	55925	0,67548	1020	0,31042	VR	VR
	55003	0,66435	1020	0,26696	VR	MS	58165	0,52048	1185	0,082186	VR	MS	58165	0,52048	1185	0,082186	VR	MS
	58356	0,70485	1020	0,22918	VR	FR	59981	0,72447	1020	0,18869	VR	FR	59981	0,72447	1020	0,18869	VR	VR
	40620	0,49062	1020	0,3076	VS	GF	44020	0,53169	1020	0,25652	VS	MG	44020	0,53169	1020	0,25652	VS	VS
	53223	0,64285	1020	0,23265	VS	FR	35721	0,1212	1924	0,41127	VS	MG	35721	0,1212	1924	0,41127	VS	MG
	24726	0,29865	1020	0,61244	VS	FR	43072	0,52024	1020	0,2918	VS	MG	43072	0,52024	1020	0,2918	VS	VS
	46046	0,55616	1020	0,30515	VT	FR	42447	0,51269	1020	0,34921	VT	MG	42447	0,51269	1020	0,34921	VT	VS
	62170	0,75091	1020	0,17668	VT	FR	46441	0,41811	1181	0,33369	VT	VS	46441	0,41811	1181	0,33369	VT	VT
	3	2,3562	4	0,94281	VT	FR	2	6,2832	2	0,86603	VT	GF	2	6,2832	2	0,86603	VT	VT

Figure 13: Identification results with 30 test data using thresholding, otsu, thresholding + otsu

From the results of testing the thresholding, otsu, thresholding + otsu can be shown in Table 3.

Table 3: Accuracy Results

The amount of data	Thresholding		Otsu		Thresholding + Otsu	
	T	F	T	F	T	F
30	8	22	15	15	21	9
Accuracy :	27%		50%		70%	

IV. CONCLUSION

The conclusion from this study the selection of the use of segmentation methods after image processing is very influential on the results of testing accuracy. Proof has been carried out in this study using the combination of

thresholding + otsu can improve accuracy results. The difference between the value of accuracy using the combination method of thresholding + otsu with thresholding reaches 43% and 20% when using the combination method of thresholding + otsu with the otsu method.

Further research is needed to select the feature extraction method where the use of the feature extraction method can be combined with other methods with the aim of further improving the accuracy of the identification of malaria parasites and their staging on thin blood smear images.

REFERENCES

- [1] Kemenkes RI, "Bukusaku Penatalaksanaan Kasus Malaria," *Kementrian Kesehatan Republik Indonesia*, vol. 1, 2017.
- [2] Kemenkes RI, "Epidemiologi Malaria di Indonesia," *Bul. Jendela Data dan Inf. Kesehat.*, vol. 1, pp. 1–16, 2011.
- [3] Kemenkes RI, "Pusat Data Dan Informasi Penyakit Malaria 2016." pp. 1–7, 2016.
- [4] A. Kumar, A. Choudhary, P.U. Tembhare, and C.R. Pote, "Enhanced Identification of Malarial Infected Objects using Otsu Algorithm from Thin Smear Digital Images," *Int. J. Latest Res. Sci. Technol.*, vol. 1, no. 2, pp. 159–163, 2012.
- [5] V. Waghmare and S. Akhter, "Image Analysis Based System for Automatic Detection of Malarial Parasite in Blood Images," *Int. J. Sci. Res. ISSN (Online Index Copernicus Value Impact Factor)*, vol. 14, no. 7, pp. 2319–7064, 2013.
- [6] M. Imran Razzak and H. Informatics, "Automatic Detection and Classification of Malarial Parasite," *Int. J. Biometrics Bioinforma.*, no. 9, p. 1, 2015.
- [7] R. Rosnelly, S.R.I. Hartati, E.D.I. Winarko, and S.R.I. Mulatsih, "Identification of Malaria Disease and Its," *J. Theor. Appl. Inf. Technol.*, vol. 95, no. 3, pp. 700–710, 2017.
- [8] S.A. Ganesh and S. Anjali, "Detection of Malarial Parasite from Blood Smear Image," *Int. Biannually J. Biomed. Lett.* 2018, vol. 4, no. 1, pp. 24–33, 2018.
- [9] C.P. McCormack, A.C. Ghani, and N.M. Ferguson, "Fine-scale modelling finds that breeding site fragmentation can reduce mosquito population persistence," *Commun. Biol.*, vol. 2, no. 1, pp. 1–11, 2019.
- [10] K. Gavina, E. Arango, C.A. Larrotta, A. Maestre, and S. K. Yanow, "A sensitive species-specific reverse transcription real-time PCR method for detection of *Plasmodium falciparum* and *Plasmodium vivax*," *Parasite Epidemiol. Control*, vol. 2, no. 2, pp. 70–76, 2017.
- [11] C. Delahunt, M.P. Horning, B.K. Wilson, J.L. Proctor, and M.C. Hegg, "Limitations of haemozoin-based diagnosis of *Plasmodium falciparum* using dark-field microscopy," *Malar. J.*, vol. 13, no. 1, pp. 1–10, 2014.
- [12] U. Salamah et al., "Segmentation of malaria parasite candidate from thick blood smear microscopic images using watershed and adaptive thresholding," *J. Telecommun. Electron. Comput. Eng.*, vol. 10, no. 2–4, pp. 113–117, 2018.
- [13] N. Ahirwar and B. Acharya, "Advanced Image Analysis Based System for Automatic Detection and Classification of Malarial," *Int. J. Inf. Technol. Knowl. Manag.*, vol. 5, no. 1, pp. 59–64, 2012.
- [14] L.M. Wein and M. Baveja, "Using fingerprint image quality to improve the identification performance of the U.S. Visitor and Immigrant Status Indicator Technology Program," *Proc. Natl. Acad. Sci. U. S. A.*, vol. 102, no. 21, pp. 7772–7775, 2005.
- [15] A. Loddio, C. Di Ruberto, and M. Kocher, "Recent advances of malaria parasites detection systems based on mathematical morphology," *Sensors (Switzerland)*, vol. 18, no. 2, pp. 1–21, 2018.
- [16] F.T. dan I.S. Suardi, "Blood Parasite Identification using Feature Based Recognition, International Conference on Electrical Engineering and Informatics," *Int. Conf. Electr. Eng. Informatics*, Bandung, 2011.
- [17] R.S.Z. May, Aziz, SSAM., "Automated Quantification and Classification of Malaria Parasites in Thin Blood Smears," *Int. Conf. Signal Image Process. Appl.*, 2013.
- [18] D. Anggraini, A.S. Nugroho, C. Pratama, and I.E. Rozi, "Automated Status Identification of Microscopic Images Obtained from Malaria Thin Blood Smears," *Int. Conf. Electr. Eng. Informatics, ICEEI 2011*, Bandung, Indonesia, no. 17–19 July, 2011.
- [19] B.R. Gonzalez, R.C., Woods, R.E., & Masters, "Digital Image Processing Using Matlab - Gonzalez Woods & Eddins." 2013.

- [20] L.M. Wein and M. Baveja, "Using fingerprint image quality to improve the identification performance of the U.S. Visitor and Immigrant Status Indicator Technology Program," *Proc. Natl. Acad. Sci. U.S.A.*, vol. 102, no. 21, pp. 7772–7775, 2005.
- [21] O. Nina, B. Morse, and W. Barrett, "A recursive otsu thresholding method for scanned document binarization," 2011 IEEE *Work. Appl. Comput. Vision, WACV 2011*, pp. 307–314, 2011.
- [22] C. Mehanian, M. Jaiswal, C. Delahunt, and C. THOMPson, "Computer-Automated Malaria Diagnosis and Quantitation Using Convolutional Neural Networks," *Proc. ICCVW, Venice, Italy*, pp. 116–125, 2017.
- [23] H.A. Nugroho, A. Darajatun, I. Ardiyanto, and R.L.B. Buana, "Classification of Plasmodium Malaria and Plasmodium Ovale in Microscopic Thin Blood Smear Digital Images," vol. 8, no. 6, pp. 2301–2307, 2018.
- [24] P. Pandit and A. Anand, "Artificial Neural Networks for Detection of Malaria in RBCs," <https://arxiv.org/ftp/arxiv/papers/1608/1608.06627.pdf>, 2016.
- [25] M. Poostchi, K. Silamut, R.J. Maude, S. Jaeger, and G. Thoma, "Image analysis and machine learning for detecting malaria," *Transl. Res.*, vol. 194, pp. 36–55, 2018.
- [26] A. Rahman et al., "Improving Malaria Parasite Detection from Red Blood Cell using Deep Convolutional Neural Networks," <https://arxiv.org/ftp/arxiv/papers/1907/1907.10418.pdf>, pp. 1–33, 2019.
- [27] S. Afkhami, "Detection of Malarial Parasite in Blood Images by two classification Methods: Support Vector Machine (SVM) and Artificial Neural Network (ANN)," *IJOCIT*, vol. 5, no. 2, pp. 81–92, 2017.
- [28] V.K. Bairagi and K.C. Charpe, "Comparison of Texture Features Used for Classification of Life Stages of Malaria Parasite," vol. 2016, 2016.
- [29] H. Chiroma et al., "Malaria severity classification through Jordan-elman neural network based on features extracted from thick blood smear," *Neural Netw. World*, vol. 25, no. 5, pp. 565–584, 2015.
- [30] M.I. Razzak, "Malarial Parasite Classification using Recurrent Neural Network," *Int. J. Image Process.*, no. 9, pp. 69–79, 2015.
- [31] N.A. Seman, N. Ashidi, M. Isa, L.C. Li, and Z. Mohamed, "Classification Of Malaria Parasite Species Based On Thin Blood Smears Using Multilayer Perceptron Network," *Sch. Electr. Electron. Eng. Univ. Sains Malaysia, Eng. Campus*, 14300, Nibong Tebal, Pulau Pinang, Malaysia, pp. 46–52.
- [32] S. Srivastava, L. Sharma, V. Sharma, A. Kumar, and H. Darbari, "Prediction of diabetes using artificial neural network approach," *Lect. Notes Electr. Eng.*, vol. 478, no. 12, pp. 679–687, 2019.
- [33] J. Kittler, 1986, Feature Selection and Extraction, in *Handbook of Pattern Recognition and Image Processing*, Tza Y. Young, King Sun Fu Ed. Academic Press
- [34] Fausett, L., 1994, *Fundamentals of Neural Networks*, Prentice Hall, Inc